Planetary and Space Science 74 (2012) 146–155

Contents lists available at SciVerse ScienceDirect

Planetary and Space Science

journal homepage: www.elsevier.com/locate/pss

Kinetic simulations of finite gyroradius effects in the lunar plasma environment on global, meso, and microscales

Esa Kallio [a,*], Riku Jarvinen [a], Sergey Dyadechkin [a], Peter Wurz [b], Stas Barabash [c], Francisco Alvarez [d], Vera A. Fernandes [e,b], Yoshifumi Futaana [c], Ari-Matti Harri [a], Jyri Heilimo [a], Charles Lue [c], Jakke Mäkelä [a,f], Niko Porjo [a,f,g], Walter Schmidt [a], Tero Siili [a]

[a] Finnish Meteorological Institute, Helsinki, Finland
[b] University of Bern, Bern, Switzerland
[c] Swedish Institute of Space Physics, Kiruna, Sweden
[d] Arquimea Ingeniería S.L, Leganés, Spain
[e] Museum für Naturkunde, Berlin, Leibniz-Institut für Evolutions- und Biodiversitätsforschung an der Humboldt-Universität zu Berlin, Germany
[f] Nokia Oyj, Finland
[g] University of Turku, Finland

ARTICLE INFO

Article history:
Received 13 March 2012
Received in revised form
11 September 2012
Accepted 13 September 2012
Available online 28 September 2012

Keywords:
The Moon
The solar wind
Moon-solar wind interaction
Magnetic anomalies
Potential sheath
Kinetic simulation

ABSTRACT

The recent *in situ* particle measurements near the Moon by Chandrayaan-1 and Kaguya missions as well as the earlier observation by the Lunar Prospector have shown that the Moon-solar wind interaction is more complicated than believed earlier. The new observations have arisen the need for a detailed modelling of the near surface plasma-surface processes and regions near the lunar magnetic anomalies. Especially, interpretation of ion, electron, and energetic neutral atoms (ENA) observations have shown that the plasma cannot be treated as a single fluid but that kinetic effects have to be taken into account.

We have studied the kinetic effects and, especially, the role of finite gyro-radius effects at the Moon by kinetic plasma simulations at three different length-scales which exist in the Moon-solar wind interaction. The solar wind interaction with a magnetic dipole, which mimics the lunar magnetic anomalies in this study, is investigated by a 3D self-consistent hybrid model (HYB-Moon) where protons are particles and electrons form a charge neutralizing mass less fluid. This study shows that the particle flux and density and the bulk velocity of the solar wind protons that hit the lunar surface just above the dipole are decreased compared to their undisturbed values. In addition, a particle ‘‘halo’’ region was identified in the simulation, a region around the dipole where the proton density and the particle flux are higher than in the solar wind, qualitatively in agreement with energetic hydrogen atom observations made by the Chandrayaan-1 mission.

The near surface plasma within the magnetic anomaly within a Debye sheath is studied by an electromagnetic Particle-in-Cell, PIC, simulation (HYB-es). In the PIC simulation both ions and electrons are treated as particles. Further, we assume in the PIC simulation that the magnetic anomaly blocks away all solar wind particles and the simulation contains only photo-electrons. The analysis shows that the increased magnetic field decreases the strength of the electric potential and results in a thinner potential sheath than without the magnetic field. Overall, the simulations give support for the suggestions that kinetic effects play an important role on the properties of the lunar plasma environment.

1. Introduction

Several new *in situ* observations have shown that the lunar plasma environment is much more complicated and interesting than earlier believed. On the charged particle (ions and electrons) and energetic neutral atoms (ENAs) point of view especially the recent measurements from Kaguya and Chandrayaan-1 missions have provided new insight of the plasma processes near the lunar surface. Kaguya had Electron Spectrum Analyzer (MAPPACE ESA), Ion Mass Analyzer (MAPPACE IMA), Ion Energy Analyzer (MAPPACE IEA), Lunar MAGnetometer (MAPLMAG) and Lunar Radar Sounder (LRS) (see e.g. Nishino et al., 2010). Chandrayaan-1 had on-board an energetic neutral atom instrument (CENA, see. e.g. Wieser et al., 2010) and ion spectrometer (SARA) (see, e.g. Lue et al., 2011). These

* Corresponding author. Tel.: +358 29539 4636.
E-mail address: Esa.Kallio@fmi.fi (E. Kallio).

0032-0633/$ - see front matter © 2012 Elsevier Ltd. All rights reserved.
http://dx.doi.org/10.1016/j.pss.2012.09.012

new detailed observations of ions (see e.g. Saito et al., 2008; Holmström et al., 2010; Lue et al., 2011), electrons (e.g. Harada et al., 2012) and ENAs (see e.g. Wieser et al., 2009) have shown that one has to take into account the motion of individual charged particles in order to interpret the observations near the lunar surface and magnetic anomalies.

The new observations have arisen the need for a detailed kinetic modelling of ions and electrons near the Moon. Generally speaking, a dedicated self-consistent plasma model for the Moon has to take into account several key elements affecting the Moon–solar wind interaction. The properties of the lunar plasma environment are affected by the Moon, the Sun and the nearby space. The Moon does not have a noticeable global intrinsic magnetic field and it does not have an atmosphere. Therefore charged particles originating from the Sun and outside of the Solar System can freely hit the lunar surface. The Sun is the source of the solar wind, a continuous flow of ions (mainly protons, H^+, and alpha particles, He^{++}) and electrons. The Sun is also the source of the interplanetary magnetic field (IMF), magnetising the solar wind plasma. The Sun also emits extreme ultraviolet (EUV) radiation that ionises both the lunar surface and neutral atoms above the surface.

The interaction of the external plasma and radiation with the Moon determines the properties of the charged particles, ions and electrons, and, consequently, the electric and magnetic fields of the lunar environment (e.g. Halekas et al., 2010a). The electric field, in turn, lifts charged dust particles (see e.g. Nitter et al., 1998), creating a heavy charged particle population with variable charge, acting as a source and sink of electrons (e.g. Stubbs et al., 2011). The properties of the plasma near the Moon have various spatial and temporal variations. For example, variations are due to (1) local lunar magnetic anomalies (e.g., Lin et al., 1998; Purucker and Nicholas, 2010), (2) as a result of the Moon revolving around the Earth (during which the Moon passes through various plasma regions in the Earth's magnetosphere and during which the solar illumination conditions on the lunar surface vary) and (3) temporal variations in the Sun and, consequently, variations in solar UV radiation (see, e.g. Sternovsky et al., 2008, and references therein) and in the solar wind.

Modelling of the properties of the lunar plasma environment is, therefore, a challenging task because a fully comprehensive self-consistent model should include all major plasma populations, electric and magnetic fields, and dust particles. Modelling is also complicated by the fact that the electric conductivity of the lunar surface is not well established. Moreover, local effects caused by geography (craters, slopes, hills etc.) and the magnetic anomalies are neither well known. Modelling of the regions near the lunar North and South poles is especially challenging because of the varying illumination conditions with the associated change in surface charging, and because of the nearby lunar plasma wake (see e.g. Farrell et al., 2007). Modelling is further complicated by temporal variability and the wide range of spatial scales involved, both in terms of the plasma physics scales and the size of the regions where they occur, which in the lunar environment often are comparable.

Presently, we focus on study of the finite gyroradius effects near the lunar plasma environments associated with the motion of ions and electrons around the magnetic field. In the solar wind the charged particles rotate around the interplanetary magnetic field (IMF). Near the lunar surface also the magnetic field associated with the lunar magnetic anomalies affects the motion and the velocity of the charged particles within their range of influence. We use two kinetic models to illustrate and to study finite gyroradius effects near the lunar plasma environment at three different length scales: (1) the "global length scale" where the modelled region includes the whole Moon, (2) the "mesoscale" where the modelled region includes a magnetic dipole and (3) the "microscale" that contains a thin photo-electron sheath above the lunar surface.

In the global scale and mesoscale case the term kinetic effect refers in this paper to the phenomena associated with the finite ion gyroradius effects because these length scales are modelled by hybrid models where ions are particles while electrons form a massless charge neutralizing fluid. Earlier hybrid model calculations for three dimensional (3D) models (e.g. Kallio, 2005; Wang et al., 2011; Holmström et al., 2010, 2012) and 2D models (e.g. Birch and Chapman, 2002; Trávníček et al., 2005) have shown to provide new insights in the investigation of the lunar plasma environment, especially when the lunar tail region has been investigated. Before the availability of hybrid models the solar wind interaction with the magnetic anomalies was studied by 2D magnetohydrodynamic (MHD) models (Harnett and Winglee, 2000) and 2D kinetic models (Harnett and Winglee, 2002). Recently, the solar wind interaction with a Moon-like conducting obstacle was studied with a Vlasov model (Umeda, 2012).

The detailed analysis of properties of photo-electrons within a strong magnetic anomaly is done by an electrostatic full Particle-in-Cell (PIC) simulation where both ions and electrons are modelled as particles and where the magnetic field is kept constant during the simulation. Such a small spatial scale, which is referred to as the microscale in this paper, cannot be modelled by a hybrid model because it assumes quasi-neutrality which is not a valid assumption within the Debye sheath near the lunar surface. A PIC simulation without a magnetic field has recently been used to study various aspects of the lunar plasma environment in 1D and 2D, including dust particles (Poppe and Horányi, 2010). Further, the electrostatic PIC approach enables us to study finite gyroradius effects of both ions and electrons.

The goal of the paper is twofold. First, to give a brief summary of several kinetic effects near the Moon and, especially, the role of the magnetic field which causes charged particle gyromotion around the magnetic field lines. Second, to study the effects of the magnetic field on the particles and fields near and within a lunar magnetic anomaly by applying two kinetic models, by a hybrid model and a PIC model. The current paper is organized as follows: first, the main characteristic features of the lunar plasma environment are introduced; second, the basic properties of the hybrid and PIC model are presented. After that the models are used to study finite gyroradius effects at three length scales. Finally the limitations and consequences of the results are discussed.

2. Lunar plasma environment

Fig. 1 summarises some of the major particle and field aspects of the lunar plasma environment. The Sun is the source of protons (H^+_{sw}) and electrons (e^-_{sw}), and sunlight ionises the lunar surface, causing photo-electron emissions and charging of its surface. In addition, the impacts of ions and electrons onto the surface result in secondary ion and electron emissions. Part of the solar wind particles can be reflected away from the surface due to the electric and magnetic fields. Near the lunar surface the length scale for the electric potential sheath, or the Debye sheath, is the Debye length, λ_D ($=\sqrt{\in_0 kT_e/n_e e^2}$, where $\in_0$ is the electric permittivity, k is the Boltzmann constant, T_e is the temperature of electrons, n_e is the density of electrons and e is the unit charge). The focus of this paper is to study the finite gyroradius effects when the charged particles rotate around the magnetic field lines of both the IMF and, near certain regions on the lunar surface, of the lunar magnetic anomaly fields.

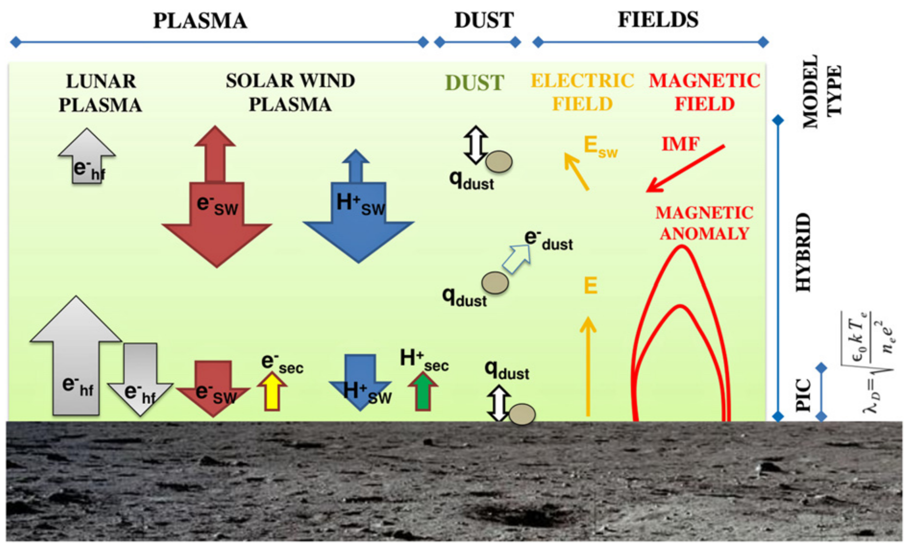

Fig. 1. A schematic illustration of plasmas and fields which affect the lunar plasma environment near the lunar surface: photo-electrons (e^-_{hf}), solar wind electrons (e^-_{sw}), electrons from the dust particles (e^-_{dust}), dust particles (q_{dust}) solar wind protons (H^+_{sw}), secondary electrons (e^-_{sec}), secondary ions (H^+_{sec}), the electric field (**E**) and the magnetic field. Because of the non-zero magnetic field associated with the interplanetary magnetic field ($\mathbf{B}_{SW}$), electric currents in the plasma and the lunar magnetic anomalies, the charged particle makes gyromotion around the magnetic field. The electric field contains the convective electric field of the solar wind ($\mathbf{E}_{sw}$) and the electric field associated with the charge separation within the potential sheath and possible also within magnetic anomalies. The length scale of the potential sheath is the Debye length (λ_D). As marked on the right hand side of the figure, in this paper a PIC simulation is used to model near surface region while a hybrid model is used to study the region within and above the magnetic anomaly. See text for details.

3. Description of the models

The kinetic models used in this paper are implemented in the HYB modelling platform which was initially created to include several hybrid models to study the solar wind interaction with various Solar System objects: HYB–Mercury for the Mercury–solar wind interaction (Kallio and Janhunen, 2003), HYB–Venus for the Venus–solar wind interaction (Kallio et al., 2006), HYB–Moon for the Moon–solar wind interaction (Kallio, 2005), HYB–Mars for the Mars–solar wind interaction (Kallio and Janhunen, 2002), HYB–Ceres for an asteroid–solar wind interaction (Kallio et al., 2008) and HYB–Titan to study Saturn's moon Titan (Kallio et al., 2004). Recently a full 3D electromagnetic PIC code was included into the HYB platform (HYB-em) (Pohjola and Kallio, 2010). More details about hybrid models, PIC simulations in general and how they compare to the magnetohydrodynamic (MHD) approach can be found elsewhere (see, e.g. Ledvina et al., 2008; Kallio et al., 2011) and only the basic features of the hybrid and PIC approaches are introduced here. The new model in the HYB platform implemented for this paper is a full kinetic 1D electrostatic PIC code (HYB-es).

3.1. Hybrid model: HYB–Moon

Several technical details of the 3D hybrid model HYB can be found elsewhere (Kallio and Janhunen, 2003). Here we focus on the basic physical assumptions and equation in a hybrid model approach.

In the hybrid simulation ions are modelled as particles, while electrons form a massless charge neutralizing fluid. When the ions are accelerated by the Lorentz force alone the equation of the motion of ions is

$$m_i d\mathbf{v}_i/dt = q_i(\mathbf{E}+\mathbf{v}_i \times \mathbf{B}) \quad (1)$$

$$d\mathbf{r}_i/dt = \mathbf{v}_i \quad (2)$$

where m_i, q_i, $\mathbf{v}_i$ and $\mathbf{r}_i$ are the mass, electric charge, the velocity and the position of an ion, **E** is the electric field vector and **B** is the magnetic field vector.

The electric field is derived from the electron momentum equation, which for the one-ion species situation (H^+) used in the present study has the form

$$\mathbf{E} = -\mathbf{U}(H^+) \times \mathbf{B}+\mathbf{j} \times \mathbf{B}/(en(H^+))+\eta\mathbf{j} \quad (3)$$

where $\mathbf{U}(H^+)$ and $n(H^+)$ are the bulk velocity and the density of protons, **j** is the electric current ($\mathbf{j}=\nabla \times \mathbf{B}/\mu_0$), η is the electric resistivity of the plasma, e is the unit charge. In Eq. (3) the plasma is assumed to be quasi-neutral, i.e., $n(H^+)=n(e^-)$. The resistivity η is taken to be constant within the simulation domain to introduce diffusion in the magnetic field propagation. This means that in the global scale simulation (Section 4.1) the IMF magnetic field diffuses through the Moon.

The magnetic field is propagated by using Faraday's law

$$d\mathbf{B}/dt = -\nabla \times \mathbf{E} \quad (4)$$

In the global scale HYB-Moon simulation the size of the simulation region was $-6R_{Moon} < x < 2R_{Moon}$; $-2R_{Moon} < y < +2R_{Moon}$ and $-2R_{Moon} < z < +2R_{Moon}$, where the solar wind flows to the $-x$ direction, the IMF points along the $+y$ and the z-axis completes the right hand coordinate system. The solar wind parameters were: (1) density (n_{sw}): 7 cm^{-3}; (2) velocity ($\mathbf{U}_{sw}$): $(-430, 0, 0)$ km/s; (3) proton temperature (T_{sw}): 0.8×10^5 K; and (4) interplanetary magnetic field ($\mathbf{B}_{sw}$): (0, 6, 0) nT. The size of the cubic shaped grid cells were $dx=dy=dz=R_{Moon}/10 \sim 174$ km. The time step (dt) in the simulation was kept small, $dt=11$ ms, to ensure the numerical stability of the solution. The average number of macro particles within a grid cell in the undisturbed solar wind was 30 in the simulations.

In the mesoscale HYB–Moon simulation the size of the simulation box was 0 km $< x <$ 200 km; -200 km $< y, z, < +200$ km. The coordinate system was as follows. The magnetic dipole was below the surface at $(x, y, z)=(-50, 0, 0)$ km, where the dipole axis was along the z-axis. The magnetic field on the surface above the dipole at the point $(x, y, z)=$ (0, 0, 0) was $(0, 0, -96)$ nT. The solar wind entered into the simulation box at $x=200$ km. The solar wind parameters were: $n_{sw}=7$ cm^{-3}; $\mathbf{U}_{sw}=(-430, 0, 0)$ km/s; $T_{sw}=0.8 \times 10^5$ K; $\mathbf{B}_{sw}=(0, 6, 0)$ nT. The size of the cubic shape grid cells were $dx=dy=dz=200$ km/30$\sim$6.7 km and dt was 0.44 ms.

The average number of macro particles within a grid cell in the undisturbed solar wind was again 30 in the simulation.

The hybrid model is self-consistent, that is, the electric field (Eq. (3)) and the magnetic field (Eq. (4)) in the simulation are derived from bulk plasma parameters in the simulation. The fields in the simulation in turn affect the motion of ions and electrons. One major advantage of the approach is that the ion velocity distribution can be modelled fully 3D and a Maxwellian velocity distribution function does not need to be prescribed, as is the case in a MHD model. Moreover, the approach includes automatically ion gyroradius effects because the ions are modelled as particles that feel the Lorentz force $q_i(\mathbf{E}+\mathbf{v}_i\times\mathbf{B})$ as they move in the plasma environment (Eq. (1).

3.2. Particle-in-Cell model: HYB–es

The microscale simulations are made by a one dimensional (1D) Particle-in-Cell (PIC) model. The characteristic feature of the physics within the Debye sheath is the charge separation between ions and electrons. This plasma region, where charge neutrality is not given, can be modelled by a PIC simulation where both ions and electrons are modelled as particles. The equations of motion of ions (index i) and electrons (index e) accelerated by the Lorentz force are

$$m_i d\mathbf{v}_i/dt = q_i\,(\mathbf{E}+\mathbf{v}_i\times\mathbf{B})+m_i\mathbf{g} \text{ and } m_e d\mathbf{v}_e/dt = e\,(\mathbf{E}+\mathbf{v}_e\times\mathbf{B})+m_e\mathbf{g} \tag{5}$$

$$d\mathbf{r}_i/dt=\mathbf{v}_i;\ d\mathbf{r}_e/dt=\mathbf{v}_e \tag{6}$$

where $\mathbf{g}$ is the gravitation acceleration on the surface of the Moon. The role of the gravitation in the PIC simulations presented in the paper is insignificant but gravitation was included anyhow for completeness.

In the PIC simulation, HYB-es, the electric field is derived from Gauss law

$$\nabla\cdot\mathbf{E}=\rho/\in_0=e(n(H^+)-n(e^-))/\in_0 \tag{7}$$

where ρ is the total charge density. At the beginning of the simulation the electric field was assumed to be zero so there is no ambient electric field and all electric field was associated with the charge separation shown in Eq. (7). The HYB-es model is an electrostatic PIC model where the magnetic field is a pre-given field, which remains unchanged during a simulation run. For a comparison, in the electromagnetic PIC simulation (see, e.g. Pohjola and Kallio, 2010) the time dependency of the magnetic field would have been derived from Eq. (4).

In the PIC simulation the simulation box was built of $dx=dy=dz=0.1$ m grid cells containing 1000 grid cells in the x direction. The surface was at $x=0$. The outer boundary was set as $x=100$ m which is sufficiently far from the surface that all photo-electrons remain within the simulation box. The analysed situation contains only photo-electrons which are formed at the surface, $x=0$. Three constant magnetic field cases $\mathbf{B}=(0, 0, B_0)$ for the magnetic anomalies were compared, where B_0 was 0, 300 nT, and 500 nT, respectively. The boundary condition was that the electric field is zero at $x=100$ m and above it. The simulation time step was 0.06 μs. For comparison, the gyroperiod of electrons, $T_g=2\pi m_e/(e\,B)$, in the 300 nT and 500 nT magnetic fields is 119 μs and 71.5 μs, respectively. The gyroradius of electrons, $r_g=m_e v_e/(eB)$, depends on the velocity of electrons and on the magnetic field. In the 500 nT magnetic field, for example, the gyroradius is 0.014 m, 0.14 m, 1.4 m and 16.54 m for the velocities of 1 km/s, 10 km/s, 100 km/s and 1452 km/s (=6 eV), respectively.

The HYB-es model includes one spatial dimension (x) and two velocity components (v_x, v_y). The velocity is propagated by Eq. (5). The velocities are used to propagate the position x in Eq. (6) and keeping y and z to their initial values (zero), which can be understood as a projecting the trajectory of an ion on the xy-plane to the x-axis.

The purpose of the HYB-es model runs was not to make a detailed study of the electric potential at some specific solar illumination conditions, solar activity periods or some specific mineral compositions of the surface. However, the simplified 1D photo-electron velocity distribution function, $f_{hf}(v_x)$, was required to have two characteristic features. First, f_{hf} does not include a long high velocity tail compared to the Maxwellian velocity distribution function (see, e.g. Grard and Tunaley, 1971). This is because the energy of a photo-electron is smaller than the energy of the solar photon from where the photo-electron gets its energy. Therefore, in the HYB-es model the energy of photo-electrons was assumed to be always less than 6 eV. Secondly, the flux of photo-electron current, j_{hf}, at the Moon surface – derived experimentally from the lunar fines exposed to solar radiation with normally incident sunlight – can be written as $j_{hf}=\cos(\Theta)4.5\ \mu A/m^2$ (Nitter et al., 1998) where Θ is the angle between the direction of the sunlight and the normal of the surface. Thus, in this simulation it is expected that j_{hf} should be of the order of $\mu A/m^2$. Therefore, the following 1D Maxwellian velocity distribution function was used, where the high energy tail was omitted

$$\begin{aligned} f_{hf}(v_x) &= F\exp\left(-v_x^2/v_{th}^2\right), && E<6\ \text{eV}\\ f_{hf}(v_x) &= 0, && E>6\ \text{eV} \end{aligned} \tag{8}$$

The HYB-es model also allows to use a 2D velocity distribution function, but 2D or 3D photo-electron velocity distribution functions are not known. In Eq. (8) the thermal velocity of electrons, v_{th}, was chosen to be 6.21×10^5 m/s (=2.2 eV) which mimics roughly the shape of the measured photo-electron velocity spectra (see, Poppe and Horányi, 2010; Fig. 1). The normalization constant F in Eq. (8) was chosen such that the photo-electron emission flux is 1×10^{-13} 1/s/m^2 corresponding to the photo-electron current of 1.6 μA/m^2.

When the HYB-es code was tested by using the Maxwellian velocity distribution function for photo-electrons, and by comparing the results to the analytical solution (Grard and Tunaley, 1971), it was found to be in good agreement between the simulation and the analytical model. Moreover, the validity of the electrostatic assumption was tested by calculating the induced magnetic field from the simulation result, which is associated with the photo-electron current in the cases where B_0 was non-zero. It was found that this induced magnetic field was several orders of magnitude smaller than the used constant magnetic field B_0, as required in the electrostatic approach.

4. Kinetic effects

In this section the 3D hybrid and 1D electrostatic PIC models were used (as described in Section 3) to study kinetic effects. The focus of this section is to study finite gyroradius effects at mesoscales (Section 4.2) and at microscales (Section 4.3) but it is first important to point out several gyroradius effects at the global scale (Section 4.1).

4.1. Global scale: The Moon–solar wind interaction and trajectories of pick-up ions

The analysis of the global length scale is based on the global 3D hybrid model (HYB–Moon), which has been used earlier to study the lunar plasma tail (Kallio, 2005). However, in the present study our goal is not to use the HYB–Moon model for a detailed analysis of the lunar wake, but to use it to illustrate basic properties of the Moon-solar wind interaction and the properties of the lunar pick-up ions.

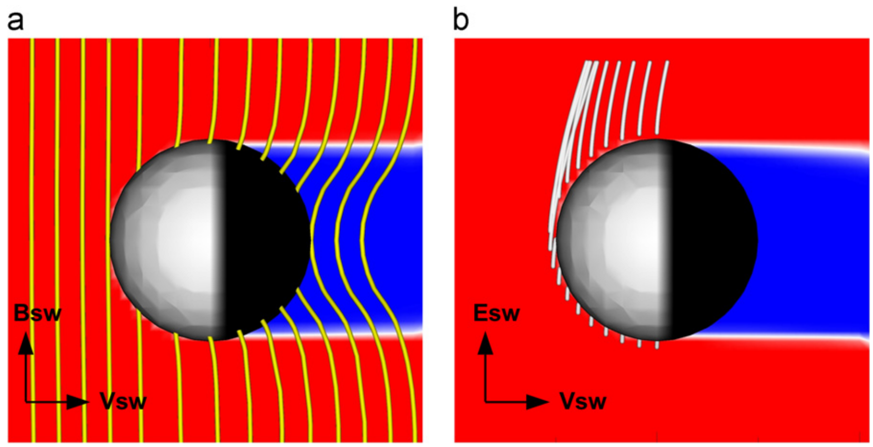

Fig. 2. (a) Illustration of the basic features of the interaction between the Moon and the undisturbed solar wind: No bow shock is formed in the solar wind plasma, magnetic field lines are diffusing through the object and a low density plasma tail is formed behind the Moon. (b) Several trajectories of O^+ pick up ions, which are formed slightly above the lunar surface, as an illustration of the finite gyroradius effect. Note the large gyroradius of the pick-up O^+ ions compared with the radius of the Moon. The 3D plasma model is a hybrid model (HYB–Moon). The colour plane shows the density of the solar wind protons: The density is near the nominal value in the red colour regions and smaller than the nominal density in the blue colour region behind the Moon. (For interpretation of the references to colour in this figure legend, the reader is referred to the web version of this article.)

Fig. 2a shows the situation when the Moon is in the solar wind. An important feature is that no bow shock is formed in front of the Moon, that is, the Moon is not a conducting obstacle against the solar wind. In the so called Earth-type solar wind interaction the global intrinsic magnetic field of the object results in a magnetosphere and a bow shock is formed. This is the case for Mercury, the Earth, and giant planets Jupiter, Saturn, Uranus and Neptune. In the so called Venus-type solar wind interaction the object has an atmosphere and planetary ions are borne by the ionising solar extreme ultraviolet (EUV) light, and an ionosphere is formed. The ionosphere deflects the solar wind flow around the object and forms a bow shock. The Moon does not have an atmosphere but only an exosphere where the neutral density is not high enough to form a highly conducting ionosphere. The Moon does not have a significant global intrinsic magnetic field either. One can also envisage that had the electric conductivity of the Moon been high, the electric currents induced inside the Moon by the solar wind could be strong enough to prevent the solar wind impacting directly on its surface (see, e.g. Johnson and Midgley, 1968). That cannot, however, take place because of the low electric conductivity of the lunar interior. As a result, the Moon is an archetype of the so called Moon-like interaction (a planetary body without an atmosphere and magnetic field) where the solar wind can directly hit against the surface of the object. The Moon–like solar wind interaction where the IMF field lines diffuse through the object is illustrated in Fig. 2a.On the global length scale, kinetic effects affect the motion of the lunar pick-up ions. These ions originate either from the lunar exosphere or from the surface and have been observed to have a clear asymmetry associated with the finite ion gyroradius effects (see e.g. Mall et al., 1998). In Fig. 2b this effect is illustrated by launching a few O^+ ions at the $y=0$ plane on the dayside 100 km above the surface. These O^+ test particles illustrate that the gyroradius of O^+ ions in the solar wind is much larger than the radius of the Moon. The ions start to move toward the direction of solar wind convection field $+E_{sw}$. Because of the large gyroradii of the ions, their trajectories form fairly straight lines in the region shown in Fig. 2b. Therefore, O^+ ions that are formed on the arc in the $z<0$ hemisphere hit against lunar surface while O^+ ions formed on the opposite hemisphere escape to space.

4.2. Mesoscale: Ion deflection by magnetic anomalies

Fig. 2 gives an oversimplified picture of the Moon-solar wind interaction as in reality the lunar magnetic anomalies affect the motion of ions and electrons. The goal of this section is to study a region near a magnetic anomaly with a hybrid model. In the model, the simulation box contains the magnetic anomaly and the incident solar wind. The grid size is small enough to resolve the main characteristics of the protons interacting with the magnetic field of the anomaly.

In this mesoscale simulation the finite ion gyroradius effects are studied near a dipolar lunar magnetic anomaly by a hybrid model. As described in Section 3.2, the mesoscale simulation is built to study the basic properties of the solar wind interaction with a magnetic anomaly by assuming that there is a local magnetic dipole below the lunar surface. The solar wind and the IMF are set to flow against the magnetised surface region and the solar wind particles are removed from the simulation when they hit the surface at $x=0$.

Fig. 3a shows the bulk flow streamlines of the solar wind protons and the density of the solar wind protons on two perpendicular planes. One plane is on the surface of the Moon at $x=0$ and another plane is perpendicular the surface at $y=0$. The streamlines do not show much deviation from the incident solar wind, except at the region above the magnetic dipole close to the surface. Moreover, just above the dipole the solar wind density is smaller than in the solar wind. Around this low density region there is an enhanced proton density region, a density "halo".

The streamlines shown in Fig. 3a are derived from the macroscopic bulk velocity ($\mathbf{U}(H^+)$) and they do not show how individual protons are moving. In Fig. 3b the trajectory of 400 solar wind H^+ ions were studied by launching test particles above the surface at $x=190$ km in the region $-30\text{ km}<y, z<30$ km. The ions had initial velocity corresponding to the solar wind ($\mathbf{U}_{sw}=(-430, 0, 0)$ km/s) and they were followed until they hit the surface at $x=0$ or moved out of the simulation box. Fig. 3b shows that the gyroradius of protons is large compared with the size of the magnetic anomaly and, therefore, the solar wind protons are non-magnetised outside of the magnetic anomaly. The red lines in Fig. 3b show protons that had the ending pointing of their trajectories above the surface at region $x>10$ km and, thus, have been reflected by the magnetic anomaly back into the upstream solar wind. Thirty eight of the launched 400 protons, approximately 10%, were reflected back. This value is in the middle of the reported range of ion reflections at magnetic anomalies (Lue et al., 2011). As can be seen in Fig. 3b, the trajectories above the magnetic anomaly are relatively straight and

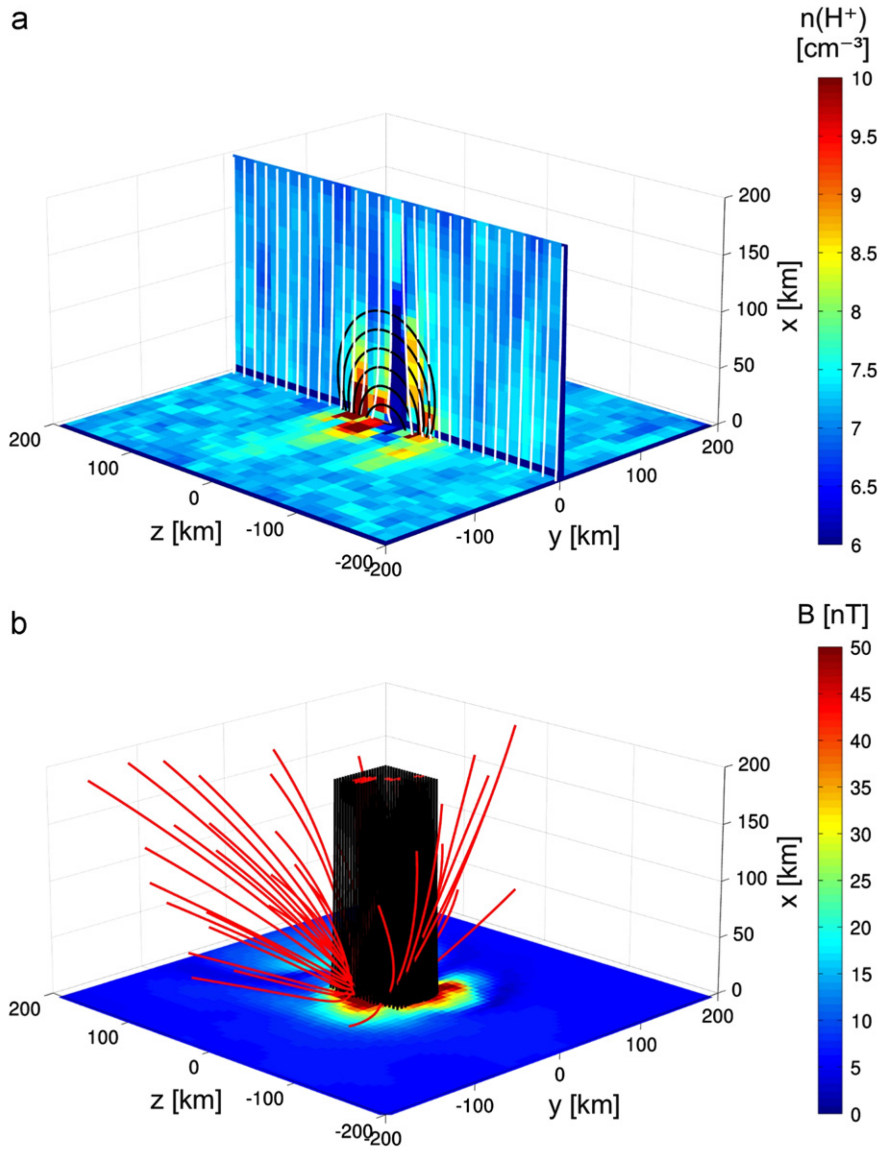

Fig. 3. Solar wind interaction with a magnetic dipole embedded in the lunar surface, which is used as a simple model for the lunar magnetic anomalies. Panel (a) shows the streamlines of the solar wind protons. The density of the solar wind protons in the horizontal and vertical plane is given by the colour code. The tracing of the streamlines was started on a line 200 km above the surface. Panel (b) shows the trajectory of 400 proton test particles which were launched above the surface at $x = 190$ km in the region -30 km $< y, z < 30$ km. The colour of the trajectory is black if the ion hits the surface and red if the ion is reflected back upstream due to the magnetic anomaly and does not hit the surface. The colour on the lunar surface ($x = 0$) shows the magnitude of the magnetic field. (For interpretation of the references to colour in this figure, the reader is referred to the web version of this article.)

no clear gyromotion around the magnetic field is visible. Indeed, this is expected to be the case in the meso length scale, because the gyroradius of protons associated with the thermal speed of the solar wind is about 100 km, that is, about the size of the simulation box. Note that a MHD simulation could not model the reflected protons because the velocity distribution function of protons is highly non-Maxwellian.

Ion trajectories shown in Fig. 3a indicate how the density "halo", a region of enhanced density of protons in Fig. 3a, is formed: The "halo" consists of protons whose original trajectories are deflected by the magnetic field anomaly and which are temporarily "packed" against the dipolar field. Moreover, inside the "halo" there is a low density region because only a few solar wind protons can enter within the region just above the dipole. In some sense this "mini-magnetosphere" region resembles the Earth's magnetosphere: The low density centre region corresponds to the Earth's magnetosphere and the higher density region to the Earth's magnetosheath. This analogy cannot, however, be continued further because there is no bow shock around the "mini-magnetosphere" as is the case in the Earth's magnetosphere because the size of the gyroradius of protons is in the same order, or larger, than the whole interaction regions of the mini-magnetosphere.

The bulk properties of the plasma on the lunar surface are studied in more detail in Fig. 4, where the impact flux, the density, the velocities and the magnetic field at the surface are shown. Fig. 4b shows density at the surface where the "cavity" and the density "halo" population on the surface are easily identified. Fig. 4c shows the bulk velocity of protons perpendicular to the surface (U_x), which decreases when the distance from the dipole decreases. This is in good agreement with the observation (see Wieser et al., 2009) where the magnetic anomalies were best seen at high particle energies when observed by energetic neutral atoms. The lower plasma speed at the magnetic anomaly is probably also a kinetic effect associated with the fact that most of the protons are reflecting away from the high magnetic field region, which results in decreasing bulk velocity component of

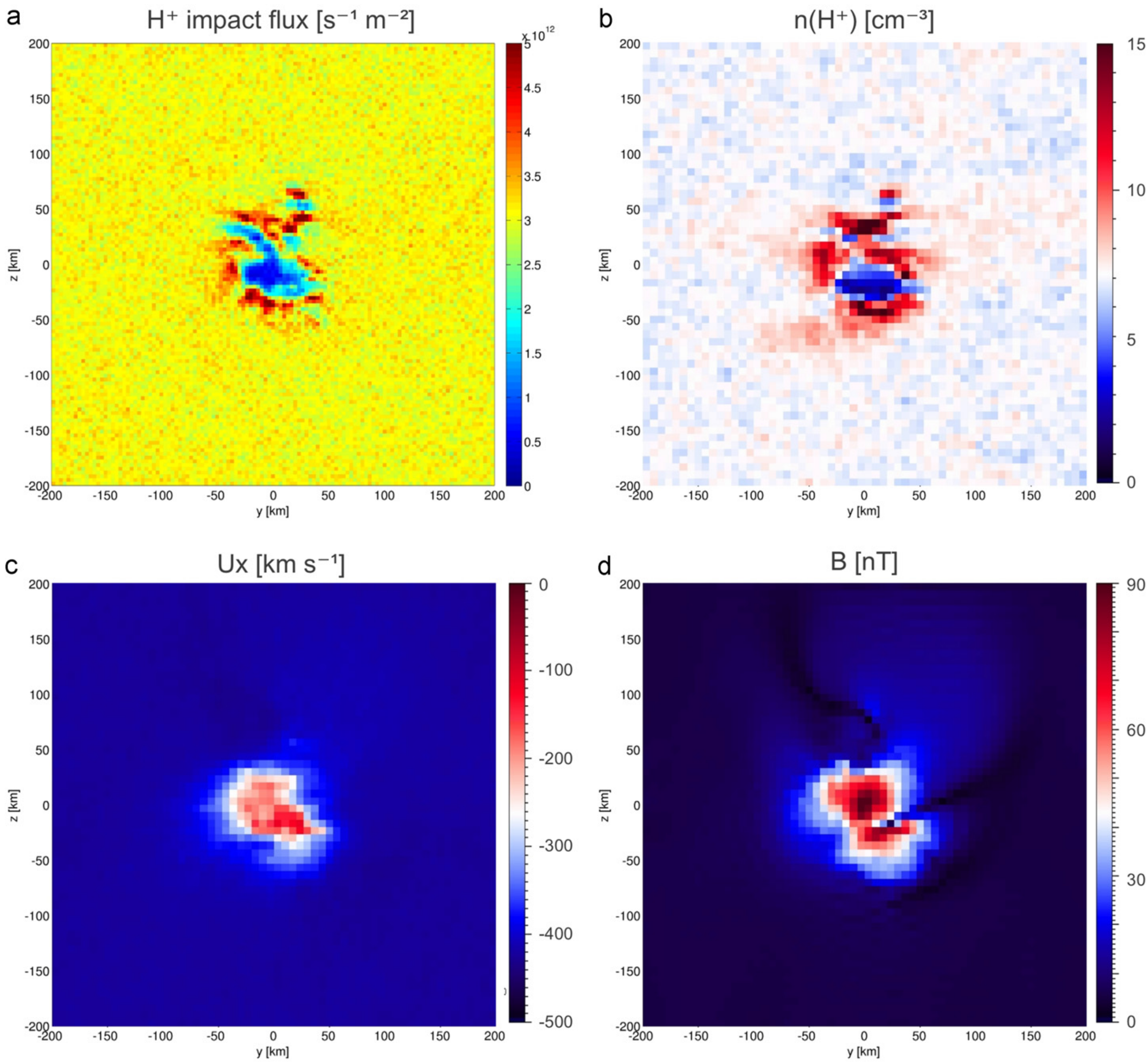

Fig. 4. Properties of the solar wind protons on the lunar surface near a magnetic dipole: (a) the impact flux of protons to the surface [s^{-1} m^{-2}], (b) the density of protons at the surface [cm^{-3}], (c) the vertical velocity of protons [km s^{-1}] and (d) the total magnetic field [nT]. The magnetic dipole is located 50 km below the surface at $y=z=0$. Note how the impact flux, the particle density and the vertical velocity are low just above the dipole. Around the dipole there is a ‘‘halo'' where the impact flux and the density of protons are higher than in the undisturbed regions far from the dipole ($\sqrt{(x^2+y^2)} > 50$ km). The total magnetic field differs from the dipolar field because of the magnetic field associated with the electric currents around the magnetic anomaly.

ions toward the surface. The small downward speed and the low plasma density result in a low particle flux onto the surface at and near the magnetic anomaly (Fig. 4a) and a flux enhancement, i.e., ‘‘flux halo'', around the low flux region which is associated with deflection of protons by the magnetic anomaly. Again, this is in good qualitative agreement with the observation by (Wieser et al., 2009). Finally, note that the total magnetic field near the magnetic dipole (Fig. 4d) is a combination of the initial dipolar field and the magnetic field associated with the ‘‘minimagnetopause currents'' around the magnetic anomaly. The magnitude and shape of the total magnetic field depend on the direction of the magnetic dipole with respect to the direction of the IMF as well as the relative strengths of the IMF and the magnetic anomaly. As a summary of Fig. 4 it can be said that the properties of the solar wind near a magnetic anomaly can differ noticeably from their undisturbed values in the interplanetary space.

4.3. Microscale: Photo-electron gyration within a magnetic field

The lunar magnetic anomaly simulation results shown in Figs. 3 and 4 imply that the density of solar wind protons and electrons near the surface above the magnetic dipole can be locally highly reduced. As a consequence, the lunar photo-electrons may form a major electron and charged particle population within the magnetic anomaly. In order to get deeper insight of such a situation where predominantly photo-electron plasma is located above a magnetic anomaly, which has generated a horizontal magnetic field, we study the properties of photo-electron plasma in the HYB-es

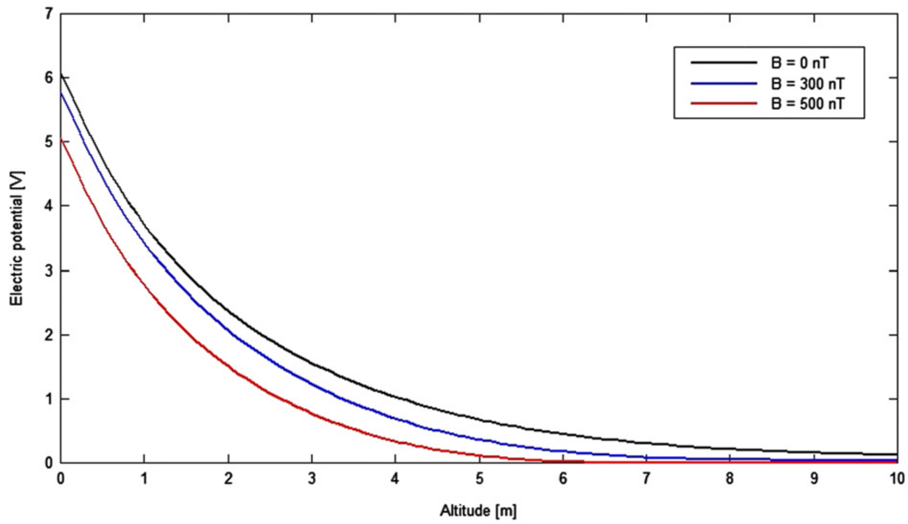

Fig. 5. Electric potential near the lunar surface at three horizontal magnetic field conditions (0 nT, 300 nT, 500 nT). Note how the increasing magnetic field results in decreasing electric potential and a less extended potential sheath region when the gyroradius becomes smaller. The simulation was made with an electrostatic PIC code (HYB-es) which contains photo-electrons.

model described in Section 3.2. In HYB-es we assume a strong horizontal magnetic field and the electric field is derived from the spatial distribution of photo-electrons.

The third spatial scale considered is the ‘‘microscale’’. In this case the length scale is on the order of the Debye length, $\lambda_D = \sqrt{\in_0 kT_e/n_e e^2}$, above the surface of the Moon. This is modelled by a full electrostatic 1D PIC code that contains one spatial dimension (height) and two velocity components (which are perpendicular to the magnetic field when the magnetic fields is not zero, see Section 3.2).Fig. 5 shows the electric potential associated with the photo-electrons when the surface magnetic field is zero and also in two magnetised cases. The magnitude of the electric potential can be seen to decrease with increasing magnetic field at the surface. Moreover, the altitude where the potential goes to zero, that is, the altitude above which photo-electrons from the surface can no longer be found in the simulation, decreases with increasing magnetic field. These affects are associated with the finite gyroradius of electrons: the higher the magnetic field value, the faster the magnetic field starts to change the initially purely vertical velocity of an electron to a horizontal velocity. This prevents an electron from entering such high altitudes as it could have reached if no magnetic field existed, and thus the altitude of the zero potential decreases. Moreover, the magnetic field returns electrons back to the surface, thus the flight time of electrons decreases, and thus the electron density. This decreases the total amount of electrons above the surface and, consequently, decreases the absolute value of electric potential. It should be recalled, however, that in a real situation also the solar wind electrons and protons exist near the lunar surface and these particles affect the properties of the photo-electrons. For example, the photo-electrons can escape from the lunar plasma environment into the solar wind (see, e.g. Poppe and Horányi, 2010).

5. Discussion

In this paper the properties of the plasma near the Moon were studied, and especially the role of the finite gyroradius effects was analysed. One of the major motivations of the study comes from the new *in situ* particle observations near the Moon. The recent lunar missions Chandrayaan-1 and Kaguya have shown that the solar wind interaction with the Moon is complex and scientifically more interesting than anticipated before, as shown by new *in situ* plasma and energetic neutral hydrogen atoms measurements.

Ion observations have shown that 0.1–1% of the incident solar wind protons are reflected back from the lunar surface from unmagnetised areas according to measurements by Kaguya (Saito et al., 2008). Moreover, measurements by Chandrayaan-1 have shown that up to 20% of the impinging solar wind protons are reflected from the lunar surface back to space as hydrogen ENAs (Wieser et al., 2009).

New observations have also triggered high interest to study the lunar magnetic anomalies. Kaguya observations suggested that over 10% of solar wind protons are reflected by the magnetic anomalies (Saito et al., 2011). Later statistical analysis based on measurements on Chandrayaan-1 found a high deflection efficiency of the solar wind protons, on average $\sim$10% but locally up to $\sim$50%, over large regions ($>$ 1000 km) of magnetic anomalies (Lue et al., 2011).

The effects of the lunar magnetic anomalies on the solar wind flow can also be seen by measuring hydrogen ENA emission from the surface. These neutrals are formed in a charge exchange process between the impacting solar wind protons and the lunar surface material. It has been shown that in the energy range from 150 eV to 600 eV, the flux of neutral hydrogen atoms was reduced to about 50% within the area of the mini-magnetosphere (Wieser et al., 2010). Since then also correlations of the shielding efficiency with solar wind plasma parameters and the field strength of the anomaly were reported (Vorburger et al., 2012). Moreover, a ring-shaped region of increased ENA flux around a mini-magnetosphere was detected (Wieser et al., 2010). The observed low flux region and the ring-shaped region (referred in this paper as a ‘‘halo’’) are in qualitative agreement with the simulation (see Fig. 4) and presented in Section 4.

The aforementioned ions and the ENA observations, and the simulations shown in this paper, also have several implications when the electric field near the lunar surface within the potential sheath is studied. First, the properties of the solar wind on the lunar surface near a magnetic anomaly can differ noticeably from their undisturbed values. Secondly, the lunar surface is a source of secondary protons when the solar wind is reflected from the lunar regolith. Third, the magnetic field influences the motion of ions and electrons within the potential sheath in microscale.

The question of how the magnetic field affects the lunar plasma environment waits, however, for more detailed modelling.

This concerns especially the magnetic anomaly modeling. The hybrid model does not contain charge separation and, consequently, no double layers. However, double layers have been suggested to play a role of the deceleration of ions and acceleration of electrons near a magnetic anomaly when the Chandrayaan-1 (Lue et al., 2011), Kaguya (Saito et al., 2012) and laboratory (Bamford et al., 2012) observations have been interpreted. Solar wind protons are also decelerated in the hybrid model and we find that the average energy of protons impacting on the surface near the magnetic anomaly is smaller than the energy of protons impacting far away from the anomaly (figure not shown). These changes of the energy of protons at magnetic anomalies found in the hybrid model are in qualitative agreement with the ENA observations, but for correct quantitative modelling they probably should be modelled by a 3D PIC model. Further, we performed test particle simulations to check the importance of a self-consistent modelling of the magnetic anomaly studied in this work. In the test particle simulations the magnetic field was assumed to contain only the pure dipole field associated with the magnetic anomaly and (i) the electric field was kept zero ($\mathbf{E}=0$) or (ii) the electric field was assumed to be the (constant) convective electric field of the solar wind ($\mathbf{E}=\mathbf{E}_{sw}$). The low density region and the "halo" region could not be identified when a similar plot as shown in Fig. 5 was made from the test particle case (figure not shown).

The properties of plasma within a magnetic anomaly can also be more complicated than in the analysed PIC model case. It is very probable that part of the solar wind protons and electrons can anyway enter within the magnetic anomaly and affect to the plasma density and the electric potential. Moreover, the electric potential structure within the magnetic anomaly can be complicated if the magnetic anomaly is shielded within a narrow electrostatic potential, as suggested by recent laboratory experiments (Bamford et al., 2012). A magnetic dipole is also a very simplified model for lunar magnetic anomalies. For example, although the Reiner Gamma magnetic anomaly (RGA) region can be approximated relative well by two magnetic dipoles (Kurata et al., 2005) in general lunar magnetic anomalies form much more complicated magnetic structures.

The strength of the anomaly magnetic fields has also strong variations from the point to point. *In situ* measurements made by Apollo indicated magnetic field strength of 3 nT–327 nT (Dyal et al., 1974). It is also notable that, based on the Lunar Prospectror electron reflectometry (LP/ER) magnetic anomaly map (Mitchell et al., 2008; Fig. 4), the magnetic field near Gerasimovich (Crisium-antipode) at $\sim 15^\circ$ South and $\sim 120^\circ$ West, is, within 30 km radius, roughly 100 nT, and within 60 km radius, roughly 30 nT, i.e., quite similar to field strengths used in the magnetic anomaly study in the Section 4 above. However, recent modelling based on LP/ER measurements suggests that the surface magnetic field strengths could reach thousands of nanotesla in some locations (Halekas et al., 2010b). This implies that a detailed magnetic anomaly study should use a dedicated magnetic anomaly map for the modelled space region.

More modelling is also required to study the role of the magnetic field in the Debye sheath. The simulations shown in this paper suggest that in the highly magnetised cases the finite gyroradius affects the electric potential within the Debye sheath when the photo-electrons are considered. Future simulations of this problem should also contain solar wind electrons and ions. The role of the direction of the magnetic field should also be varied, both the direction of the IMF and the direction of the magnetic dipole below the surface. A global simulation should also be performed in 2D or 3D.

More detailed modelling is also necessary to take into account the dust particles. As illustrated in Fig. 1, dust particles are source and sink of electrons. The dust affects therefore on the density and properties of electrons and, consequently, on the electric potential on the electric field. However, self-consistent modelling of the lunar dust-plasma environment is beyond the scope of this paper and it is a complex modelling task because one should know, for example, the size distribution of the dust particles in the plasma and its shape and electric properties. One of the major issues is also the velocity of dust particles which has to be modelled or one has to use some manually given velocity model. These important features of the lunar dust are still very poorly established. New insight into the properties of the dust particles has been obtained for recent laboratory measurements (e.g. Wang et al., 2010; Dove et al., 2011). However, more laboratory measurements and *in situ* dust measurements are needed to evaluate the role of the lunar dust for the lunar plasma environment.

Finally, it is worth to note that the plasma physical processes near the Moon in the solar wind which are analysed in this paper may take place at all airless bodies in the Solar System, such as Mercury and asteroids.

References

Bamford, R.A., Kellett, B., Bradford, W.J., Norberg, C., Thornton, A., Gibson, K.J., Crawford, I.A., Silva, L., Gargaté, L., Bingham, R., 2012. Minimagnetospheres above the lunar surface and the formation of lunar swirls. Physical Review Letters 109, 081101.

Birch, P.C., Chapman, S.C., 2002. Two dimensional particle-in-cell simulations of the lunar wake. Physics of Plasmas 9, 1785–1789.

Dyal, P., Parkin, C.W., Daily, W.D., 1974. Magnetism and the interior of the Moon. Reviews of Geophysics and Space Physics 12 (4), 568–591, http://dx.doi.org/10.1029/RG012i004p00568.

Dove, A., et al., 2011. Mitigation of lunar dust adhesion by surface modification. Planetary and Space Science 59, 1784–1790.

Farrell, W.M., Stubbs, T.J., Vondrak, R.R., Delory, G.T., Halekas, J.S., 2007. Complex electric fields near the lunar terminator: the near-surface wake and accelerated dust. Geophysical Research Letters 34, L14201, http://dx.doi.org/10.1029/2007GL029312.

Grard, R.J.L., Tunaley, J.K.E., 1971. Photoelctron sheath near planar probe in interplanetary space. Journal of Geophysical Research 76 (10), 2498–2505.

Harada, Y., et al., 2012. Nongyrotropic electron velocity distribution functions near the lunar surface. Journal of Geophysical Research 117 (A7), A07220, http://dx.doi.org/10.1029/2012JA017642.

Halekas, J.S., et al., 2010a. New views of the lunar plasma environment. Planetary and Space Science , http://dx.doi.org/10.1016/j.pss.2010.08.011.

Halekas, J.S., Lillis, R.J., Lin, R.P., Manga, M., Purucker, M.E., Carley, R.A., 2010b. How strong are lunar crustal magnetic fields at the surface? Considerations from a reexamination of the electron reflectometry technique. Journal of Geophysical Research 115, E03006, http://dx.doi.org/10.1029/2009JE003516.

Harnett, E.M., Winglee, R.M., 2000. Two-dimensional MHD simulations of the solar wind interaction with magnetic field anomalies on the surface of the Moon. Journal of Geophysical Research 105, 24997–25007.

Harnett, E.M., Winglee, R.M., 2002. 2.5D Particle and MHD simulations of mini-magnetospheres at the Moon. Journal of Geophysical Research 107 (A12), 1421, http://dx.doi.org/10.1029/2002JA009241.

Holmström, M., Wieser, M., Barabash, S., Futaana, Y., Bhardwaj, A., 2010. Dynamics of solar wind protons reflected by the Moon. Journal of Geophysical Research 115, A06206, http://dx.doi.org/10.1029/2009JA014843.

Holmström, M., Fatemi, S., Futaana, Y., Nilsson, H., 2012. The interaction between the Moon and the solar wind. Earth, Planets and Space 64, 237–245, http://dx.doi.org/10.5047/eps.2011.06.040.

Johnson, F.S., Midgley, J.E., 1968. Notes on the lunar magnetosphere. Journal of Geophysical Research 73 (5).

Kallio, E., Janhunen, P., 2002. Ion escape from Mars in a quasineutral hybrid model. Journal of Geophysical Research 107 (A3).

Kallio, E., Janhunen, P., 2003. Modelling the solar wind interaction with Mercury by a Quasineutral Hybrid Model. Annales Geophysicae 21 (11), 2133–2145.

Kallio, E., Sillanpää, I., Janhunen, P., 2004. Titan in subsonic and supersonic flow. Geophysical Research Letters 31, L15703, http://dx.doi.org/10.1029/2004GL020344.

Kallio, E., 2005. Formation of the lunar wake in quasi-neutral hybrid model. Geophysical Research Letters 32, L06107, http://dx.doi.org/10.1029/2004GL021989.

Kallio, E., Jarvinen, R., Janhunen, P., 2006. Venus–solar wind interaction: asymmetries and the escape of O^+ ions. Planetary and Space Science 54 (13–14), 1472–1481.

Kallio, E., et al., 2008. On the impact of multiply charged heavy solar wind ions on the surface of Mercury, the Moon and Ceres. Planetary and Space Science 56 (11), 1506–1516, http://dx.doi.org/10.1016/j.pss.2008.07.018.

Kallio, E., Chaufray, J.-Y., Modolo, R., Snowden, D., Winglee, R., 2011. Modeling of Venus, Mars, and Titan. Space Science Reviews , http://dx.doi.org/10.1007/s11214-011-9814-8.

Kurata, M., Tsunakawa, H., Saito, Y., Shibuya, H., Matsushima, M., Shimizu, H., 2005. Mini-magnetosphere over the Reiner Gamma magnetic anomaly region on the Moon. Geophysical Research Letters 32, L24205, http://dx.doi.org/10.1029/2005GL024097.

Ledvina, S.A., Ma, Y.-J., Kallio, E., 2008. Modeling and simulating flowing plasmas and related phenomena. Space Science Reviews 139 (1–4), http://dx.doi.org/10.1007/s11214-008-9384-6.

Lin, R.P., Mitchell, D.L., Curtis, D.W., Anderson, K.A., Carlson, C.W., McFadden, J., Acuña, M.H., Hood, L.L., Binder, A., 1998. Lunar surface magnetic fields and their interaction with the solar wind: results from Lunar Prospector. Science 281 (5382), 1480–1484, http://dx.doi.org/10.1126/science.281.5382.1480.

Lue, C., Futaana, Y., Barabash, S., Wieser, M., Holmstrom, M., Bhardwaj, A., Dhanya, M.B., Wurz, P., 2011. Strong influence of lunar crustal fields on the solar wind flow. Geophysical Research Letters 38, L03202, http://dx.doi.org/10.1029/2010GL046215.

Mall, U., Kirsch, E., Cierpka, K., Wilken, B., Söding, A., Neubauer, F., Gloeckler, G., Galvin, A., 1998. Direct observation of lunar pick-up ions near the Moon. Geophysical Research Letters 25 (20), 3799–3802, http://dx.doi.org/10.1029/1998GL900003.

Mitchell, D.L., Halekas, J.S., Lin, R.P., Frey, S., Hood, L.L., Acuña, M.H., Binder, A., 2008. Global mapping of lunar crustal magnetic fields by Lunar Prospector. Icarus 194, 401–409, http://dx.doi.org/10.1016/j.icarus.2007.10.027.

Nishino, M.N., et al., 2010. Effect of the solar wind proton entry into the deepest lunar wake. Geophysical Research Letters 37, L12106, http://dx.doi.org/10.1029/2010GL043948.

Nitter, T., Havnes, O., Melandso, F., 1998. Levitation and dynamics of charged dust in the photoelectron sheath above surface in space. Journal of Geophysical Research 103 (A4), 6605–6620, http://dx.doi.org/10.1029/97JA03523.

Pohjola, V., Kallio, E., 2010. On the modeling of planetary plasma environments by a fully kinetic electromagnetic global model HYB-em. Annales Geophysicae 28, 743–751 ⟨www.ann-geophys.net/28/743/2010/⟩.

Poppe, A., Horányi, M., 2010. Simulations of the photoelectron sheath and dust levitation on the lunar surface. Journal of Geophysical Research 115, A08106, http://dx.doi.org/10.1029/2010JA015286.

Purucker, M.E., Nicholas, J.B., 2010. Global spherical harmonic models of the internal magnetic field of the Moon based on sequential and coestimation approaches. Journal of Geophysical Research 115, E12007, http://dx.doi.org/10.1029/2010JE003650.

Saito, Y., et al., 2008. Solar wind proton reflection at the lunar surface: Low energy ion measurement by MAPPACE onboard SELENE (KAGUYA). Geophysical Research Letters 35, L24205, http://dx.doi.org/10.1029/2008GL036077.

Saito, Y., et al., 2011. Inflight performance and initial results of Plasma Energy Angle and Composition Experiment (PACE) on SELENE (KAGUYA). Space Science Reviews 154 (1–4), 265–303, http://dx.doi.org/10.1007/s11214-010-9647-x.

Saito, Y., et al., 2012. Simultaneous observation of the electron acceleration and ion deceleration over lunar magnetic anomalies. Earth, Planets and Space 64, 83–92, http://dx.doi.org/10.5047/eps.2011.07.011.

Sternovsky, Z., Chamberlin P., Horanyi M., Robertson S., Wang X., 2008. Variability of the lunar photoelectron sheath and dust mobility due to solar activity. Geophysical Research Letters, 113, A10104, http://dx.doi.org/10.1029/2008JA013487.

Stubbs, T.J., Glenar, D.A., Farrell, W.M., Vondrak, R.R., Collier, M.R., Halekas, J.S., Delory, G.T., 2011. On the role of dust in the lunar ionosphere. Planetary and Space Science , http://dx.doi.org/10.1016/j.pss.2011.05.011.

Trávníček, P., Hellinger, P., Schriver, D., Bale, S.D., 2005. Structure of the lunar wake: two-dimensional global hybrid simulations. Geophysical Research Letters, 32, http://dx.doi.org/10.1029/2004GL022243.

Umeda, T., 2012. Effect of ion cyclotron motion on the structure of wakes: a Vlasov simulation. Earth, Planets and Space 64 (2), 231–236.

Vorburger, A., Wurz, P., Barabash, S., Wieser, M., Futaana, Y., Holmström, M., Bhardwaj, A., Asamura, K., 2012. Energetic neutral atom observations of magnetic anomalies on the lunar surface. Journal of Geophysical Research 115, E12007, http://dx.doi.org/10.1029/2010JE003650.

Wang, X., Horányi, M., Robertson, S., 2010. Investigation of dust transport on the lunar surface in a laboratory plasma with an electron beam. Journal of Geophysical Research 115, A11102, http://dx.doi.org/10.1029/2010JA015465.

Wang, Y.-C., Müller, J., Ip, W.-H., Motschmann, U., 2011. A 3D hybrid simulation study of the electromagnetic field distributions in the lunar wake. Icarus 216, 415–425, http://dx.doi.org/10.1016/j.icarus.2011.09.021.

Wieser, M., et al., 2009. Extremely high hydrogen reflection from Planetary regolith in space. Planetary and Space Science 57, 2132–2134, http://dx.doi.org/10.1016/j.pss.2009.09.012.

Wieser, M., et al., 2010. First observation of a mini magnetosphere above a lunar-magnetic anomaly using energetic neutral atoms. Geophysical Research Letters 37, L05103, http://dx.doi.org/10.1029/2009GL041721.